Multiorbital bosons in bipartite optical lattices

Jani-Petri Martikainen[1,2] and Jonas Larson[3,4]
[1]*Aalto University, P.O. Box 1510, FIN-00076 Aalto, Finland*
[2]*NORDITA, S-10691 Stockholm, Sweden*
[3]*Department of Physics, Stockholm University, S-10691 Stockholm, Sweden*
[4]*Institut für Theoretische Physik, Universität zu Köln, Köln, D-50937, Germany*
(Received 20 March 2012; published 10 August 2012)

We study interacting bosons in a two-dimensional square bipartite optical lattice. By focusing on the regime where the first three excited bands are nearly degenerate (i.e., the first-excited p bands in one sublattice are nearly degenerate with the s band of the other sublattice), we derive a multi-orbital tight-binding model which captures the most relevant features of the band structure. In addition, we also derive a corresponding generalized Bose-Hubbard model and solve it numerically under different situations, both with and without a confining trap. It is especially found that the hybridization between sublattices can strongly influence the phase diagrams and, in a trap, enable even appearances of condensed phases intersecting the same Mott insulating plateaus.

DOI: 10.1103/PhysRevA.86.023611 PACS number(s): 03.75.Lm, 03.75.Mn

I. INTRODUCTION

The understanding that Hubbard models can be realized with ultracold atoms in optical lattices [1] has stimulated extensive effort to explore different aspects of quantum many-body physics in optical lattices [2,3]. The early works focused on the lowest-energy band and, in a pioneering experiment by Greiner *et al.* [4], the Mott-superfluid transition with ultracold bosons was observed. More recently, experimental groups have started to probe the properties of ultracold atoms under circumstances where the excited energy bands [5] can no longer be ignored. This is most relevant since it has been demonstrated that the emerging multi-orbital effects can indeed have crucial effects also on the ground-state phase diagrams [6]. These excited bands can become important either when the atom-atom interactions become very large [7–14] or when atoms are deliberately prepared in the excited bands. Such "out-of-equilibrium–state" preparation has been established by using accelerating lattices [15] or Raman transitions between bands [16]. In the realm of these new experiments, one hopes to explore the regime where metastable excited many-body states show very different properties from those of the ground state [17–23].

The experiment most closely relevant for our purposes is the one by Wirth *et al.* [24]. Bosonic atoms were prepared in the ground state of a bipartite optical lattice and then the lattice was suddenly changed so that the initial ground-state–band atoms became (quasi) degenerate with a set of other bands which were initially separated by a large band gap. This process drove atoms into bands with nontrivial orbital properties and enabled the observation of superfluidity on these so-called p bands. This experiment was followed by others [25,26] where unconventional superfluidity was observed in the even-more-excited f bands.

Motivated by these experiments and especially on the aspects of the physics when different bands become degenerate, we study multiband bosons in a bipartite square lattice when bands cross. Such band crossing can imply topologically nontrivial band structures [27,28]. In principle, with the help of artificial gauge fields, such band structures can also be engineered on the lowest band [29,30], but they might be easier to engineer in the excited bands were artificial gauge fields may become unnecessary. For example, in a square bipartite lattice the band structure can be composed of flat bands intersecting Dirac cones which, on the one hand, have interesting analogs with graphene physics, but the flat bands also have interesting influences on the dynamical properties of the gas [31,32]. The physics of Dirac fermions have been studied in square optical lattices also in the absence of the flat band [33].

As in the experiment by Wirth *et al.* [24], we consider a bipartite square lattice of deep $\mathcal{A}$ sites and more shallow $\mathcal{B}$ sites which, however, have a higher energy offset. Under such circumstances, the excited (localized) states in $\mathcal{A}$ sites can become resonant with the ground states in $\mathcal{B}$ sites. When this happens, the p bands can be strongly hybridized with the d band. For vanishing atom-atom interaction, most of the relevant physics is captured by a tight-binding (TB) model, which predicts the existence of Dirac points and a flat band. Proceeding by adding atom-atom interactions, we derive a generalized multiband Bose-Hubbard model. We solve this theory from weak to strong interactions as well as in a trap. The calculated solutions reveal transitions from incompressible Mott insulators to condensed phases, but due to different atom-atom interactions the Mott lobes can be very dissimilar from those predicted by the usual single-band Bose-Hubbard model. Furthermore, the solution in a trap reveals the possibility that condensed states in different sublattices occur in different regions of the trap. Our findings complement some other very recent ones, like Ref. [34] where p-band bosons in a shallow bipartite optical lattice in terms of a nonlinear boson model are studied, and the work [35] analyzing the band structure renormalized by the presence of interactions and the condensate in the broken symmetry phase. Finally, Sun *et al.* [36] also derived a fermionic tight-binding model which is quite similar to the one used by us.

The paper is organized as follows: We begin by outlining the theory relevant for our purposes in Sec. II. In particular, Sec. II A presents the tight-binding model to describe the ideal gas of atoms and in Sec. II B we extend the model to include atom-atom interactions. In Sec. III the generalized Bose-Hubbard model is solved within the Gutzwiller ansatz approach, and in Sec. III we discuss the solution in a harmonic trap. We end with a few concluding remarks in Sec. IV.

 ©2012 American Physical Society

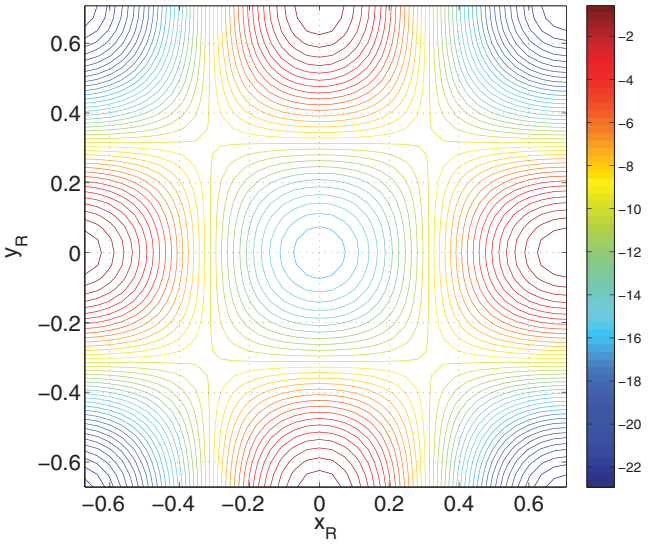

FIG. 1. (Color online) Symmetric lattice potential with $V_0 = 10E_R$ over one unit cell. The parameters were chosen as $\epsilon = \eta = 1$, $\alpha = 0$, and $\theta/\pi = 0.556$. x_R and y_R refer to coordinate axes rotated by $\pi/4$ with respect to the laboratory axes $\hat{x}$ and $\hat{y}$. The shallow $\mathcal{B}$ site is in the center while the deeper $\mathcal{A}$ sites are in the corners. Distance, $\lambda/2$, between $\mathcal{A}$ and $\mathcal{B}$ sites was taken as a unit of length.

II. THEORETICAL FORMULATION

A. Ideal system

We will assume a two-dimensional lattice potential similar to the one used in the experiments by Wirth *et al.* [24];

$$V(x,y) = -\frac{V_0}{4}|\eta\{[\hat{z}\cos(\alpha) + \hat{y}\sin(\alpha)]e^{ikx} + \epsilon\hat{z}e^{-ikx}\} + e^{i\theta}\hat{z}(e^{iky} + \epsilon e^{-iky})|^2, \quad (1)$$

where V_0 is the lattice depth, k the lattice wave number, η accounts for a small difference in the powers directed to different interferometer branches, ϵ characterizes the power reduction in the retroreflected beams due to imperfect optics, and the angle α tunes the anisotropy introduced if $\epsilon \neq 1$. The angle θ sets a relative phase between the two standing waves. $\hat{x}$, $\hat{y}$, and $\hat{z}$ are the unit vectors in the respective directions. Furthermore, the transverse $\hat{z}$ direction has been reduced due to tight confinement. We will mostly consider a symmetric lattice with $\epsilon = \eta = 1$, and $\cos(\alpha) = \epsilon$, but since different parameter choices can break the p-band degeneracies we allow for such possibilities as well. In Fig. 1 we show an example of a unit cell of this potential. Generally, the lattice is a bipartite square lattice where the two sublattices have lattice sites of different depths. Here we are interested in the parameter regime where the ground state in the shallow sites is quasiresonant with the first-excited states of the deep sites. The resulting band structure of this regime is depicted in Figs. 2(a) and 2(b). Here, and in the following, we scale the energies in terms of the recoil energy $E_R = \hbar^2(2\pi/\lambda)^2/(2m)$ of the atoms with mass m to absorb a photon of wavelength λ. In particular, Fig. 2 is calculated for $V_0 = 10E_R$. In this region, the two lowest-excited p bands become degenerate with the d band. When this happens, nontrivial band structures with Dirac points emerge. Furthermore, one of the bands is almost flat, suggesting that interactions play a larger role for atoms prepared in this band.

Restricting our analysis to the three bands of Fig. 2 (i.e., the localized ground state in the shallow $\mathcal{B}$ sites and the first two excited states in deep $\mathcal{A}$ sites), we obtain an effective theory in terms of three different orbitals. In the absence of an external trap we can write the ideal gas Hamiltonian in momentum space as

$$H = \sum_{\mathbf{k}} \phi_{\mathbf{k}}^{\dagger} \hat{H}(k) \phi_{\mathbf{k}}, \quad (2)$$

where

$$\phi_{\mathbf{k}} = \begin{bmatrix} \hat{\psi}^{\mathcal{B}}_{s,\mathbf{k}} \\ \hat{\psi}^{\mathcal{A}}_{x,\mathbf{k}} \\ \hat{\psi}^{\mathcal{A}}_{y,\mathbf{k}} \end{bmatrix} \quad (3)$$

describes the three types of orbitals included in our theory. There is an s-like orbital in the shallow $\mathcal{B}$ sites, $\hat{\psi}^{\mathcal{B}}_{s,\mathbf{k}}$, and p-like x and y orbitals in the deep $\mathcal{A}$ sites, $\hat{\psi}^{\mathcal{A}}_{x,\mathbf{k}}$ and $\hat{\psi}^{\mathcal{A}}_{y,\mathbf{k}}$, respectively. When the energy of the s orbital in the $\mathcal{B}$ sites is close to the energy of the p orbitals in the $\mathcal{A}$ sites, the dominant tunneling process is the one hybridizing orbitals in different sublattices. This involves nearest neighbors and lower barrier height for tunneling while other tunneling processes require couplings over larger distances and are therefore greatly suppressed. Thus, for sufficiently deep lattices we can ignore tunnelings within $\mathcal{A}$ or $\mathcal{B}$ sites. On the other hand, since they only involve single-particle physics, our theory can naturally include next nearest-neighbor tunnelings easily when those are required.

In momentum space, this results in a TB model

$$\hat{H}(k) = \begin{bmatrix} E_s^{\mathcal{B}}(\mathbf{k}) & -2it_{xx}^{\mathcal{AB}}\sin(k_x) & -2it_{yy}^{\mathcal{AB}}\sin(k_y) \\ 2it_{xx}^{\mathcal{AB}}\sin(k_x) & E_x^{\mathcal{A}}(\mathbf{k}) & 0 \\ 2it_{yy}^{\mathcal{AB}}\sin(k_y) & 0 & E_y^{\mathcal{A}}(\mathbf{k}), \end{bmatrix}, \quad (4)$$

whose parameters can be deduced from the exact band-structure calculations (see Fig. 2). In the next section, this model will also be given in position space. One consequence of the hybridization can be seen in how the orbital character of the system enters, for example, in the sine terms in the above TB model. Hopping occurs between s and p orbitals, which implies that the tunneling coefficient alternates signs between neighboring sites giving rise to a sine rather than a cosine dispersion. In order to simplify notations, we choose our zero-energy level to be the energy of the s orbital in the $\mathcal{B}$ sites. Since only nearest neighbor tunneling processes are included, the momentum dependence disappears from the diagonal terms and we have $E_s^{\mathcal{B}}(\mathbf{k}) = 0$, $E_x^{\mathcal{A}}(\mathbf{k}) = E_x^{\mathcal{A}} \equiv \delta/2$, and $E_y^{\mathcal{A}}(\mathbf{k}) = E_y^{\mathcal{A}} \equiv -\delta/2$.

We note that a somewhat related TB model was also derived by Sun *et al.* [36]. However, in that model the underlying lattice potential was different and the p orbitals were degenerate while in our case they can be different to account for the possible anisotropy of $\mathcal{A}$ sites. This anisotropy was indeed an important ingredient in the experiment by Wirth *et al.* [24]. In the symmetric case with $\delta = 0$ the lowest-energy state of the TB

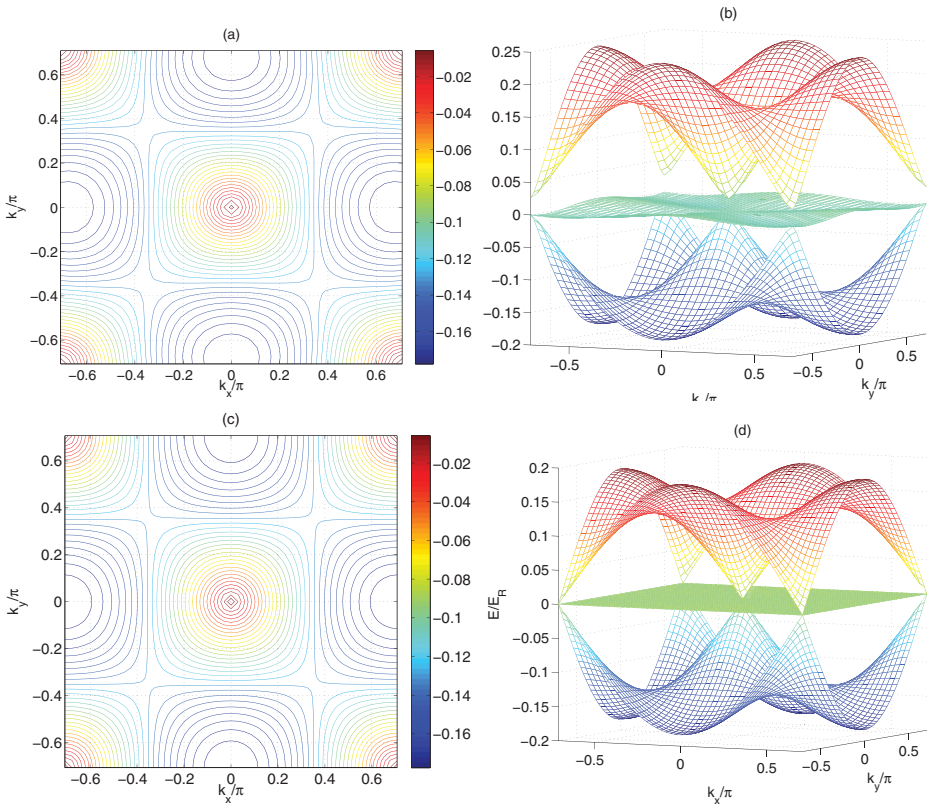

FIG. 2. (Color online) Dispersions of the three lowest excited bands. (a) and (b) are numerically calculated for a lattice with $V_0 = 10E_R$, $\epsilon = \eta = 1, \alpha = 0$, and $\theta/\pi = 0.556$. (a) shows the lowest excited band while (b) shows all three excited bands in the same plot. (c) and (d) are calculated with the TB model with parameters $t_{xx}^{AB} = t_{yy}^{AB} = 0.064\,85E_R$ and $\delta = 0$.

model is fourfold degenerate, but this degeneracy is lifted as soon as $\delta \neq 0$ so that the minima are only twofold degenerate.

Furthermore, in the symmetric case with $\delta = 0$ the sine dispersions give rise to Dirac points at the origin as well as on the edges of the first Brillouin zone at $(\pm\pi/\sqrt{2},0)$ and $(0, \pm\pi/\sqrt{2})$. A nonzero detuning δ implies an effective mass term that splits the Dirac point degeneracies. Similarly, in graphene the relativistic electrons become massive when the symmetry between the corresponding two triangular sublattices is broken [27]. Contrary to graphene, rather than having a two-level structure, the present model has three bands and the Berry phase, as a Dirac point is encircled, vanishes. The additional level appears as a flat band sandwiched between the other two bands.

$\hat{H}(k)$ of Eq. (4) has the same structure as the Hamiltonian for a Λ scheme frequently occurring in light-matter–interaction models in quantum optics, and we can directly conclude that states of the flat band correspond to dark states with zero energy. These eigenstates are superpositions of p orbitals and have a vanishing amplitude of being in the ("excited") s state in $\mathcal{B}$ sites [37]. With this in mind, by considering anisotropic lattices ($t_{xx}^{A\mathcal{B}} \neq t_{yy}^{A\mathcal{B}}$) we notice that it would be possible to apply various examples of complete or fractional *stimulated Raman adiabatic passage* schemes [38] to prepare specific orbital states for the atoms. Intriguingly, the Hamiltonian in Eq. (4) also has a clear connection to spin-orbit–coupled systems. In the long-wavelength limit we can expand the trigonometric functions and find that the coupling between orbitals is linearly proportional to momentum [39–41]. Usually, spin-orbit coupling in ultracold-atom systems is generated between different atomic hyperfine states [41,42]. Here the internal states of the atoms are not effected, but the spin-orbit–like coupling is a band-structure effect that occurs between different orbitals.

In Figs. 2(c) and 2(d) we demonstrate that the TB model above is indeed a good approximation close to band degeneracy by comparing it with the numerically calculated band structure [Figs. 2(a) and 2(b)]. As can be seen, for the symmetric lattice it reproduces the main features of the real band structure very well. Corrections beyond nearest-neighbor hopping terms is seen to give rise to higher-order variations in the dispersions mostly clear in the flat band. The tunneling coefficients $t_{xx}^{A\mathcal{B}}$ and $t_{yy}^{A\mathcal{B}}$ have been extracted from the band widths of the numerically obtained bands. While our model does work well close to resonance, it should be kept in mind that, generally, the real band structure is more complicated and more tunneling processes might have to be included in the theory.

B. Interacting system

In the previous section the ideal gas theory was derived and we now proceed by adding the atom-atom interactions. For ultracold atoms, interactions can be well modeled by contact interactions,

$$U = \frac{g}{2}\int d\mathbf{r}\hat{\psi}^\dagger(\mathbf{r})\hat{\psi}^\dagger(\mathbf{r})\hat{\psi}(\mathbf{r})\hat{\psi}(\mathbf{r}). \quad (5)$$

In a deep lattice, the field operator $\hat{\psi}(\mathbf{r})$ is naturally expanded in terms of the localized orbitals described by the Wannier wave functions $w_x^{\mathcal{A}}(x,y)$, $w_y^{\mathcal{A}}(x,y)$, and $w_s^{\mathcal{B}}(x,y)$. That is, we truncate the Hilbert space to contain only the three most relevant bands (i.e., the expansion is restricted to $\mathcal{B}$-site s orbitals and $\mathcal{A}$-site p orbitals).

In the usual way, we limit the interaction to include only the dominant onsite terms. The strengths of various interactions are proportional to the scattering length, but their relative magnitudes depend on the orbital wave functions. To estimate these strengths we approximate the onsite orbitals with harmonic oscillator wave functions and, in this way, can analytically solve the integrals describing interaction between x orbitals in $\mathcal{A}$ sites

$$U_{xx} = U_0 \int dxdy \left|w_x^{\mathcal{A}}(x,y)\right|^4, \tag{6}$$

between y orbitals in $\mathcal{A}$ sites

$$U_{yy} = U_0 \int dxdy \left|w_y^{\mathcal{A}}(x,y)\right|^4, \tag{7}$$

between x and y orbitals in $\mathcal{A}$ sites

$$U_{xy} = U_0 \int dxdy \left|w_x^{\mathcal{A}}(x,y)\right|^2 \left|w_y^{\mathcal{A}}(x,y)\right|^2, \tag{8}$$

and finally between s orbitals in $\mathcal{B}$ sites

$$U_{sB} = U_0 \int dxdy \left|w_s^{\mathcal{B}}(x,y)\right|^4. \tag{9}$$

We take that the remaining prefactor U_0 is tunable either by changing the lattice depth or by changing the effective scattering length. In the harmonic approximation $U_{xy} = U_{xx}/3$. This condition can sometimes lead to accidental degeneracies, which are removed as soon as the condition is broken [23]. However, in this work this does not play a major role. Since the shallow sites are wider than the deep sites, their orbitals are also more extended. This implies that U_{sB} is often surprisingly close to the values of U_{xx} and U_{yy} even though these involve wider excited-state orbitals. For concreteness, in the following we choose the lattice depth as $V_0 = 10E_R$, in which case it turns out that $U_{xx} = U_{yy} \approx 0.95U_{sB}$.

With the above-introduced interaction strengths, we are now in a position to write down a many-body Hamiltonian describing multi-orbital bosons in a bipartite optical lattice. The corresponding Hamiltonian takes the form

$$H_T = H_0 + H_{I,\mathcal{B}} + H_{I,\mathcal{A}}, \tag{10}$$

where

$$\begin{aligned} H_0 = {} & \frac{\delta}{2} \sum_{\mathbf{i}\in\mathcal{A}} \left(\hat{n}_{x,\mathbf{i}}^{\mathcal{A}} - \hat{n}_{y,\mathbf{i}}^{\mathcal{A}}\right) \\ & - \frac{1}{2} \sum_{\alpha\beta} \sum_{\langle \mathbf{i},\mathbf{j}_{\beta_+}\rangle} \left(t_{\alpha\beta}^{\mathcal{AB}} \hat{\psi}_{s,\mathbf{j}_{\beta_+}}^{\mathcal{B}\dagger} \hat{\psi}_{\alpha,\mathbf{i}}^{\mathcal{A}} + \text{H.c.}\right) \\ & + \frac{1}{2} \sum_{\alpha\beta} \sum_{\langle \mathbf{i},\mathbf{j}_{\beta_-}\rangle} \left(t_{\alpha\beta}^{\mathcal{AB}} \hat{\psi}_{s,\mathbf{j}_{\beta_-}}^{\mathcal{B}\dagger} \hat{\psi}_{\alpha,\mathbf{i}}^{\mathcal{A}} + \text{H.c.}\right) \\ & - \mu \sum_{\mathbf{i}\in\mathcal{A}} \left(\hat{n}_{x,\mathbf{i}}^{\mathcal{A}} + \hat{n}_{y,\mathbf{i}}^{\mathcal{A}}\right) - \mu \sum_{\mathbf{i}\in\mathcal{B}} \hat{n}_{s,\mathbf{i}}^{\mathcal{B}} \end{aligned} \tag{11}$$

describes the energy offsets and nearest-neighbor tunneling giving rise to hybridization between orbitals. Here, $\mathbf{i} = (i_x, i_y)$ labels the lattice sites and μ is the chemical potential. $\hat{n}_{x,\mathbf{i}}^{\mathcal{A}}$, $\hat{n}_{y,\mathbf{i}}^{\mathcal{A}}$, and $\hat{n}_{s,\mathbf{i}}^{\mathcal{B}}$ are the number operators for x and y orbitals in an $\mathcal{A}$ site $\mathbf{i}$ and s orbitals in a $\mathcal{B}$ site $\mathbf{i}$. The notation $\mathbf{j}_{\beta_+}$ ($\mathbf{j}_{\beta_-}$) indicates a nearest neighbor of $\mathbf{i} = (i_x, i_y)$ to the right (left) in the direction $\beta \in \{\hat{x}, \hat{y}\}$. For example, $\mathbf{j}_{x_+} = (i_x + 1, i_y)$ while $\mathbf{j}_{x_-} = (i_x - 1, i_y)$. Finally, "H.c." indicates the Hermitian conjugate. The hopping term must be written in this way since, in this case tunneling, is sensitive to the left and right difference. Intuitively, this is easy to understand by considering a p orbital with a node. This orbital wave function changes sign as one moves along the axis towards the neighboring site with s-orbital wave function. The overlap of these two wave functions is predominantly positive if the neighbor is to the left (for example), but predominantly negative if it is to the right. Note how such "space dependence" in the hopping term also appears in lattice models exposed to (synthetic) magnetic fields [41]. The tunneling parameters $t_{\alpha\beta}^{\mathcal{AB}}$ denotes the strength of tunneling of α orbitals in the $\mathcal{A}$ sublattice in the direction β into the nearest neighbor s orbital in the $\mathcal{B}$ sublattice. In the theory used here $t_{xy}^{\mathcal{AB}} = t_{yx}^{\mathcal{AB}} = 0$. In the momentum representation, the term H_0 corresponds to the TB Hamiltonian encountered in the previous subsection.

The remaining terms describe interactions.

$$H_{I,\mathcal{B}} = \frac{U_{s\mathcal{B}}}{2} \sum_{\mathbf{i}\in\mathcal{B}} \hat{n}_{s,\mathbf{i}}^{\mathcal{B}} \left(\hat{n}_{s,\mathbf{i}}^{\mathcal{B}} - 1\right) \tag{12}$$

accounts for the interactions in the $\mathcal{B}$ sites and

$$\begin{aligned} H_{I,\mathcal{A}} = {} & \sum_{\mathbf{i}\in\mathcal{A}} \left[\frac{U_{xx}}{2} \hat{n}_{y,\mathbf{i}}^{\mathcal{A}} \left(\hat{n}_{y,\mathbf{i}}^{\mathcal{A}} - 1\right) + \frac{U_{yy}}{2} \hat{n}_{y,\mathbf{i}}^{\mathcal{A}} \left(\hat{n}_{y,\mathbf{i}}^{\mathcal{A}} - 1\right)\right] \\ & + \frac{U_{xy}}{2} \left[\hat{\psi}_{x,\mathbf{i}}^{\mathcal{A}\dagger} \hat{\psi}_{x,\mathbf{i}}^{\mathcal{A}\dagger} \hat{\psi}_{y,\mathbf{i}}^{\mathcal{A}} \hat{\psi}_{y,\mathbf{i}}^{\mathcal{A}} + \hat{\psi}_{y,\mathbf{i}}^{\mathcal{A}\dagger} \hat{\psi}_{y,\mathbf{i}}^{\mathcal{A}\dagger} \hat{\psi}_{x,\mathbf{i}}^{\mathcal{A}} \hat{\psi}_{x,\mathbf{i}}^{\mathcal{A}}\right] \\ & + 2U_{xy} \hat{n}_{x,\mathbf{i}}^{\mathcal{A}} \hat{n}_{y,\mathbf{i}}^{\mathcal{A}} \end{aligned} \tag{13}$$

accounts for the interactions within the $\mathcal{A}$ sites. This term is somewhat more complicated than the corresponding term in the shallow sites since x and y orbitals interact and (for bosons) can change into one another. Finally, we note that, when $\delta = 0$, the total Hamiltonian supports a symmetry corresponding to swapping of x- and y-flavor atoms in the $\mathcal{A}$ sites.

III. GUTZWILLER RESULTS

The Gutzwiller ansatz [43] for the many-body wave functions provides a reasonably accurate description of interacting bosonic systems, especially in dimensions $D > 1$. Due to the bipartite lattice and multiple flavors in one sublattice, the approach is slightly generalized compared to that of the usual Bose-Hubbard model. The Gutzwiller ansatz we use is given by

$$|\psi\rangle = \prod_{\mathbf{i}\in\mathcal{A}} \sum_{\mathbf{n}^{\mathcal{A}}} a_{\mathbf{n}^{\mathcal{A}}}^{(\mathbf{i})} |\mathbf{n}^{\mathcal{A}}\rangle_{\mathbf{i}} \prod_{\mathbf{j}\in\mathcal{B}} \sum_{n_s^{\mathcal{B}}} b_{n_s^{\mathcal{B}}}^{(\mathbf{j})} \left|n_s^{\mathcal{B}}\right\rangle_{\mathbf{j}}. \tag{14}$$

The expansion coefficients $a_{\mathbf{n}^{\mathcal{A}}}^{(\mathbf{i})} = a_{n_x^{\mathcal{A}}, n_y^{\mathcal{A}}}^{(\mathbf{i})}$ and $b_{n_s^{\mathcal{B}}}^{(\mathbf{j})}$ are the Gutzwiller amplitudes of the corresponding onsite Fock state. For our purposes, in the $\mathcal{A}$ sites, the relevant subspace is spanned by Fock states of the form $|\mathbf{n}^{\mathcal{A}}\rangle = |n_x^{\mathcal{A}}, n_y^{\mathcal{A}}\rangle$, where

$n_\alpha^{\mathcal{A}}$ is the occupation number of the α orbital. In the $\mathcal{B}$ sites, the wave function is expanded in terms of Fock states $|n_s^{\mathcal{B}}\rangle$ associated with s orbitals. The Gutzwiller ansatz captures the onsite physics exactly, but ignores some correlations between sites. In the limit where the onsite wave functions are taken to be coherent states, it recovers the Gross-Pitaevskii limit of weakly interacting bosons. This limit is approached as interactions relative to kinetic energy become small. In the limit of strong interactions, the Gutzwiller ansatz can predict different insulating phases. Depending on the problem, the insulating states predicted by the Gutzwiller ansatz can be degenerate and these degeneracies can in principle be broken due to the weak intersite correlations not encountered for in this approach. This was demonstrated for the square and cubic lattices by treating the kinetic energy terms as perturbations [23].

Calculating the energy expectation value $\langle\psi|H_T|\psi\rangle$, using the ansatz in Eq. (14), gives us an energy functional in terms of the unknown (complex) amplitudes $a^{(\mathbf{i})}_{\mathbf{n}^{\mathcal{A}}}$ and $b^{(\mathbf{j})}_{n_s^{\mathcal{B}}}$. This energy functional must then be minimized to find the ground state. Even though this functional is very complex and the minimization is not always easy, we have found that standard conjugate gradient methods work with few caveats. First, the energy functional can have many local minima into which the minimization algorithm can become stuck and consequently fail to converge into the global minimum. In order to build up confidence in the results it is important to try different initial states. Second, the minimization algorithm might have trouble in converging to the correct phase ordering. For example, complex amplitudes give rise to different phase factors in the condensate order parameters and, in an energy minimum, these phase factors should be properly ordered throughout the lattice [24]. If the conjugate gradient method is used as a black box, it might not converge to optimal phase ordering. To get around this, it is important to impose different orderings into the initial state of the minimization routines and finally pick the solution that has the lowest energy. In the absence of a trap we find the solution in a 4×4 lattice where each sublattice has 8 sites. We use periodic boundary conditions and choose to truncate the Fock-state expansion of the Gutzwiller ansatz so that the maximum onsite occupation number is 8.

In the superfluid region we find that the ground-state phases of the condensate order parameters are arranged in the same way as discussed by Wirth *et al.* [24] for an isotropic lattice. Here, the phase of the condensate order parameter in the $\mathcal{B}$ sites changes by $\pm 2\pi$ as one moves around $\mathcal{B}$-sublattice plaquettes. Neighboring plaquettes have an opposite phase winding. In the $\mathcal{A}$ sites, the onsite order parameters are superpositions of x and y orbitals. These superposition are vortex-like states proportional to $e^{i\phi}(x \pm iy)$ and the vorticity has an opposite sign in neighboring $\mathcal{A}$ sites so that onsite angular momenta are ordered "antiferromagnetically." Similarly to the $\mathcal{B}$ sites, the phase ϕ of the prefactor $e^{i\phi}$ varies by $\pm 2\pi$ as one travels around $\mathcal{A}$ site plaquettes and neighboring plaquettes have an opposite winding of this phase factor. Far in the superfluid phase where the onsite states can be approximated by coherent states, atoms in the $\mathcal{A}$ sites can be pictured as clockwise- or counterclockwise-rotating condensates with a quantization $\langle\hat{L}_z\rangle = \pm 1$ where $\hat{L}_z$ is the angular momentum operator in the transverse z direction.

Note that the swapping symmetry of x- and y-flavor atoms implies a flip of the vorticity in each site. Closer to the insulating phases where the interaction begins to dominate, the picture is more complex and the onsite x- and y-flavor atoms can become highly entangled. While the Gutzwiller ansatz (14) is not able to predict intersite entanglement, it indeed captures such intrasite entanglement. As an example, looking at the Mott insulating phase with $n^{\mathcal{A}} = 3$ atoms in the $\mathcal{A}$ sites, the Gutzwiller method gives degenerate ground states in the $\mathcal{A}$ sites. For example, the states with $|\psi\rangle_L = \prod_{\mathbf{i}\in\mathcal{A}} a^{(\mathbf{i})}_{3,0}|3,0\rangle_{\mathbf{i}} + a^{(\mathbf{i})}_{1,2}|1,2\rangle_{\mathbf{i}}$ or $|\psi\rangle_R = \prod_{\mathbf{i}\in\mathcal{A}} a^{(\mathbf{i})}_{0,3}|0,3\rangle_{\mathbf{i}} + a^{(\mathbf{i})}_{2,1}|2,1\rangle_{\mathbf{i}}$, with $a^{(\mathbf{i})}_{3,0} = a^{(\mathbf{i})}_{0,3} \approx 0.6$ and $a^{(\mathbf{i})}_{1,2} = a^{(\mathbf{i})}_{2,1} \approx -0.8$ are degenerate. As discussed above, in the Gutzwiller method these two states are decoupled in the insulating phase and breaking the degeneracies requires an improved ansatz and/or higher-order perturbation theory in the tunneling. It is clear that these two examples of insulating states are not eigenstates of $\hat{L}_z$.

We show an example of the magnitudes of the relevant observables in the phase diagram for the isotropic case with degenerate p orbitals in Fig. 3. As is clear, the phase diagram is very different from the usual sequence of ever-lower Mott lobes corresponding to higher onsite atom numbers [44]. In our case there are insulating states with integer occupation numbers, but since interactions in different sublattices are different and the other sublattice has several flavors, the positions of the boundaries for different Mott states are not expected to be in same positions for different sublattices in the limit of weak tunneling. The hybridization of orbitals in different sublattices complicates the picture further.

This interplay between sublattices gives rise to superfluid "fingers" extending into the region where each sublattice alone would be expected to be in a Mott insulator. For example, $\mathcal{B}$ sites make a transition from 1 atom per site to 2 atoms per site at $\mu/U_{s\mathcal{B}} = 1$. This is apparent in the order parameter $\langle\hat{\psi}^{\mathcal{B}}_{s,\mathbf{i}}\rangle$ being nonzero in the narrow region around $\mu/U_{s\mathcal{B}} = 1$ even when tunneling becomes weak. With these parameters and weak tunneling the $\mathcal{A}$ sites are expected to be in an insulating state with 2 atoms per site ($|n_x^{\mathcal{A}} = 1, n_y^{\mathcal{A}} = 1\rangle$), but coupling with the condensate order parameter in the $\mathcal{B}$ sites can induce a nonzero order parameter $\langle\hat{\psi}^{\mathcal{A}}_{\beta,\mathbf{i}}\rangle$. Similar observations apply around $\mu/U_{s\mathcal{B}} \approx 1.25$ where the $\mathcal{A}$ sites undergo a transition to 3 atoms per site. This transition can induce a nonzero condensate order parameter in the $\mathcal{B}$ sites.

It should be noted that the number fluctuations in x and y flavors in the $\mathcal{A}$ sites can be nonzero even in Mott insulating regions. For example, the Mott insulating state with 3 atoms in the $\mathcal{A}$ sites is a superposition of different basis states with the total of 3 atoms per site. Only the total number of atoms is fixed to an integer value. The local order parameter breaks the time-reversal symmetry and the angular momentum in $\mathcal{A}$ sites is nonzero and equal to ± 1 in the condensed region. The angular momentum in neighboring $\mathcal{A}$ sites points in opposite directions. The nonzero value of angular momentum in the condensed phase is not surprising since the interaction energy is minimized for onsite states with $(x \pm iy)$-type vortex superpositions of p orbitals [23,45].

In Fig. 4 we show an example of the phase diagram for the anisotropic case with a p-orbital splitting $\delta/U_{sB} = 1$. In the

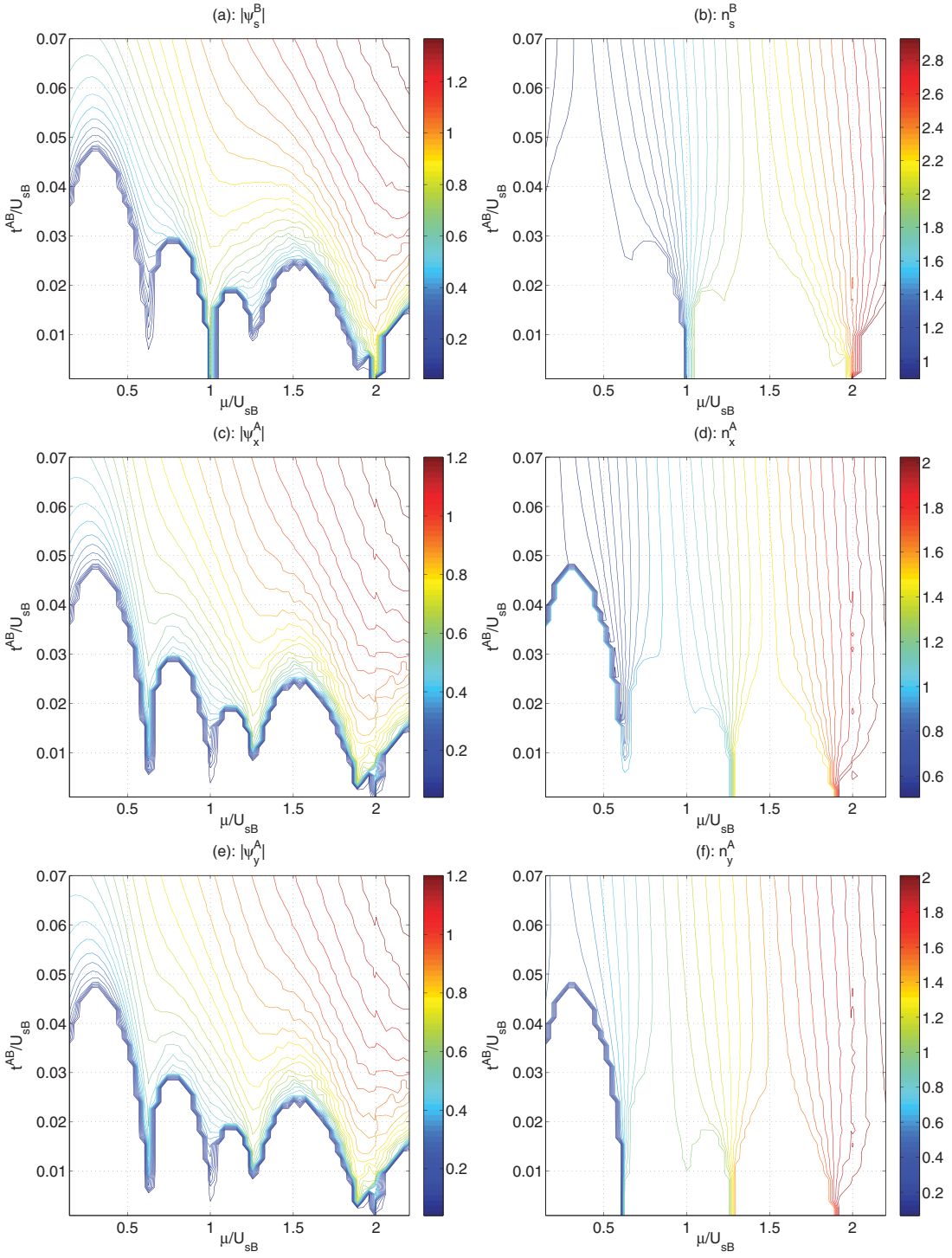

FIG. 3. (Color online) Condensate order parameters and onsite atom numbers parametrized by chemical potential and hybridization tunneling $t^{\mathcal{AB}} = t_{xx}^{\mathcal{AB}} = t_{yy}^{\mathcal{AB}}$ when p orbitals are degenerate. (However, in order to make the plot clearer we did add a very small anisotropy of $\delta = 10^{-4}$ to break the degeneracy of states in $\mathcal{A}$ sites with only one atom per site.) The left-hand plots (a), (c), and (e) display condensate densities $|\langle\hat{\psi}_{s,\mathbf{i}}^{\mathcal{B}}\rangle|^2$ and $|\langle\hat{\psi}_{\beta,\mathbf{i}}^{\mathcal{A}}\rangle|^2$ ($\beta \in \{x,y\}$), while (b), (d), and (f) show atom-flavor densities $n_{s,\mathbf{i}}^{\mathcal{B}}$ and $n_{\beta,\mathbf{i}}^{\mathcal{A}}$. The roughness that is visible, especially for higher chemical potentials, indicates the level of numerical uncertainties in these regions. (In the Mott insulating region with $n^{\mathcal{A}} = 1$ we choose $n_{x,\mathbf{i}}^{\mathcal{A}} = 1$, but since interactions do not contribute here other choices are also possible.)

superfluid regions both p orbitals are nonzero, but the order parameter (and density) for the y orbital is smaller in magnitude. In the Mott insulating regions with 1 or 2 atoms per site, the onsite interactions (with these parameters) are not strong enough to induce large fraction of atoms into the higher y orbitals and therefore only the x orbitals are substantially populated. However, as the atom number in the $\mathcal{A}$ sites increases to 3 or more the y-orbital population also becomes substantial.

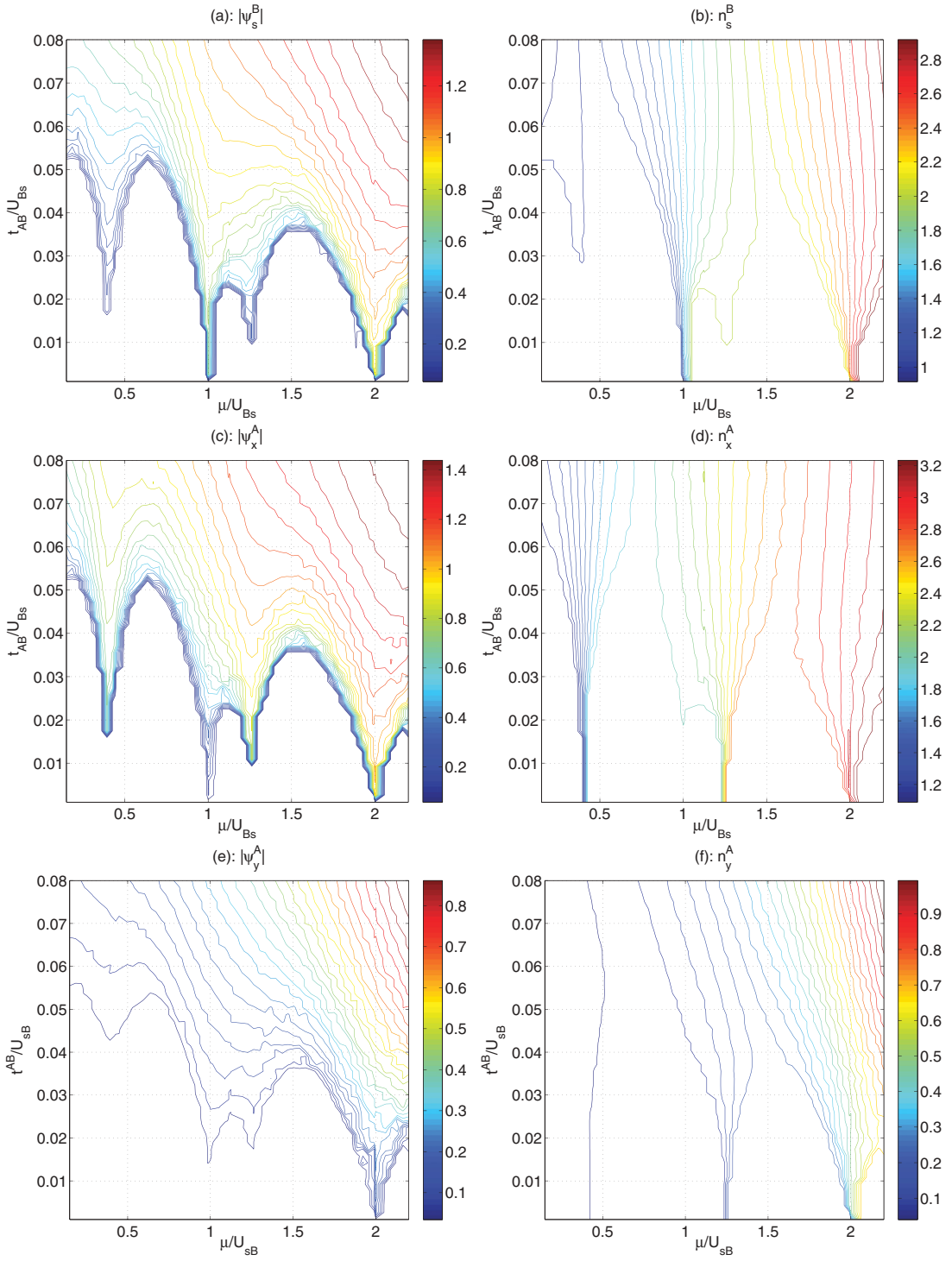

FIG. 4. (Color online) Condensate order parameters and onsite atom numbers parametrized by chemical potential and hybridization tunneling $t^{\mathcal{AB}} = t_{xx}^{\mathcal{AB}} = t_{yy}^{\mathcal{AB}}$ for the anisotropic case with $\delta/U_{s\mathcal{B}} = 1$. The plots to the left [(a), (c), and (e)] show condensate densities $|\langle\hat{\psi}_{s,\mathbf{i}}^{\mathcal{B}}\rangle|^2$ and $|\langle\hat{\psi}_{\beta,\mathbf{i}}^{\mathcal{A}}\rangle|^2$ ($\beta \in \{x,y\}$) while the ones to the right [(b), (d), and (f)] display atom-flavor densities $n_{s,\mathbf{i}}^{\mathcal{B}}$ and $n_{\beta,\mathbf{i}}^{\mathcal{A}}$. The small amount of scatter visible, especially in (e), is indicative of numerical uncertainties.

When we choose $\delta \neq 0$ we break the degeneracy of the x and y orbitals. In the limit of zero tunneling we expect that if splitting becomes in some sense large relative to onsite interactions, atoms would prefer to reside on the x orbital only. It is easy to show that with 2 atoms per $\mathcal{A}$ site, the transition occurs at $\delta = U_{xx}/3$. It is important to keep in mind that, for the case of nonzero tunneling, the situation becomes much more complex and the results may actually depend on the system size. With the Gutzwiller ansatz we find that, in the superfluid regime (we typically had $t_{xx}^{\mathcal{AB}}/U_{s\mathcal{B}} \sim 0.2$ to 0.5), the onsite angular momentum (which vanishes if only one orbital is occupied) per particle is

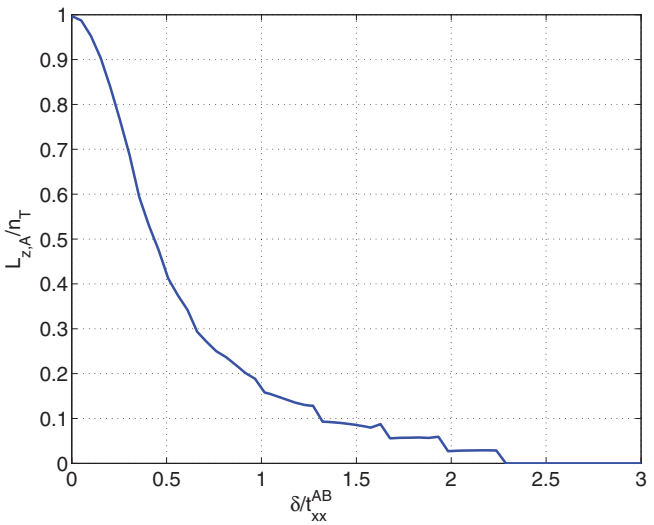

FIG. 5. (Color online) Angular momentum per particle in the $\mathcal{A}$ sites as a function of energy difference δ between p orbitals. We choose $t_{xx}^{\mathcal{AB}}/U_{s\mathcal{B}} = 0.2$, $\mu/t_{xx}^{\mathcal{AB}} = 1$, and $t_{xx}^{\mathcal{AB}}$ as the unit of energy. (The staircase structure at larger δ is due to numerical limitations in finding the global energy minimum for larger onsite atom numbers with a finite basis set.)

smoothly reduced from its value ± 1 at $\delta = 0$ to zero. This is demonstrated in Fig. 5. Vanishing onsite angular momentum is reached when $\delta/t_{xx}^{\mathcal{AB}} \sim 2$ which corresponds fairly well to what would be predicted from the onsite results with a particle number fixed to an integer value (remember that $U_{s\mathcal{B}} \approx U_{xx}$):

$$\delta/t_{xx}^{\mathcal{AB}} = (\delta/U_{s\mathcal{B}})\left(U_{s\mathcal{B}}/t_{xx}^{\mathcal{AB}}\right) \approx \tfrac{1}{3}\left(U_{s\mathcal{B}}/t_{xx}^{\mathcal{AB}}\right). \tag{15}$$

As expected, the onsite angular momentum also drops faster for larger $t_{xx}^{\mathcal{AB}}/U_{s\mathcal{B}}$ since this implies smaller onsite interaction strengths.

If we replace the operators with complex numbers ψ_α to derive a Gross-Pitaevskii equations for each orbital, we find that, for the onsite problem, the effective chemical potential and thus also the density of y orbitals vanish when $\delta/2 = \mu - U_{xy}n_x$ at which point the density of the x orbital is related to the chemical potential through $n_x = (\mu + \delta/2)/U_{xx}$. This implies that, in this limit, the transition from states with orbital angular momentum to pure x-orbital condensate happens at $\delta_c = (U_{xx} - U_{xy})n_x$, where $n_x = |\psi_x|^2$.

A. Trapped system

Typical experiments would most likely involve the presence of a confining trapping potential and, for this reason, it is important to also discuss the behavior with inhomogeneous density distributions. Our predictions for the phase diagram in a homogeneous system suggest an interesting possibility in a trap. Usually, the solution of the Bose-Hubbard model in a trap gives rise to a "wedding-cake" structure where Mott plateaus corresponding to different integer fillings are sandwiched between superfluid regions [46].

If we were to apply a local-density approximation to our system, we could think of the chemical potential as a local quantity $\mu = \mu_{\text{center}} - V_{\text{trap}}(i_x,i_y)$, where $V_{\text{trap}}(i_x,i_y)$ would typically be a harmonic trap. Traversing from the center of the cloud to its edge would correspond to moving in the phase diagram from some high value of $\mu/U_{s\mathcal{B}}$ towards zero. If the starting point is in the Mott insulating phase we could indeed have a wedding-cake structure for each sublattice, but their Mott plateaus do not always coincide. Furthermore, we can have situations when a condensate order parameter appears inside the same Mott plateau. We will next demonstrate that these simple observations are valid in a trap also beyond the local-density approximation.

We can do this within the theoretical framework used so far, but replacing the chemical potential μ with $\mu_{\text{center}} - V_{\text{trap}}(i_x,i_y)$ in the Hamiltonian in Eq. (12) and then solving the problem with the trapping potential

$$V_{\text{trap}}(i_x,i_y) = \gamma\{[i_x - (N_x+1)/2]^2 + [i_y - (N_y+1)/2]^2\}, \tag{16}$$

with N_x and N_y being the number of sites along x and y, respectively. [The minima of the harmonic potential is shifted to $((N_x+1)/2,(N_y+1)/2)$ since we choose $i_\alpha \in \{1,\ldots,N_\alpha\}$.] As an example, we choose an isotropic lattice with $t/U_{s\mathcal{B}} = 0.015$ and the chemical potential in the center $\mu_{\text{center}}/U_{s\mathcal{B}} = 1.5$ so that, in the center of the cloud, we expect the $\mathcal{A}$ sites to be in an insulating state with three atoms per site. The trap coefficient γ we choose in such a way that $\mu_{\text{center}} - V_{\text{trap}}(i_x,i_y)$ becomes negative at the edge of the lattice so that the density vanishes there.

We demonstrate the resulting ground state of the trapped bosons in Fig. 6. The bosons arrange themselves into the familiar wedding-cake structure with Mott insulating regions separated by superfluid regions. Remarkably, as suggested by the results in the absence of a trapping potential, since our system has two different sublattices with different onsite interactions, superfluid "rings" can occur in different locations for different orbitals. For example, closest to the center we have a region where the $\mathcal{A}$ sites are Mott insulators with $n^{\mathcal{A}} = n_x^{\mathcal{A}} + n_y^{\mathcal{A}} = 3$ while the $\mathcal{B}$ sites are insulating with $n^{\mathcal{B}} = 2$. The transition to an $n^{\mathcal{A}} = 2$ phase occurs via a superfluid phase in the $\mathcal{A}$ sites. However, in this region the condensate order parameter in $\mathcal{B}$ sites is still very small. Also, there is a condensed phase between regions with $n^{\mathcal{B}} = 2$ and $n^{\mathcal{B}} = 1$ while the condensate order parameters in $\mathcal{A}$ sites are negligible. Consequently, the physics predicted by using the theory without the trapping potential can also persist in trapped systems.

Recently, the trapped system of p-band bosons in a square lattice was analyzed and it was found that the density of different x- or y-orbital atoms were elongated in one direction and the symmetry of the confining trap was broken [45]. The present system is different due to the hybridization of s and p orbitals, which implies that the condensate cloud preserves the symmetry for an isotropic trap. On the other hand, if one prepares the system so that the tunneling coefficients $t_{xx}^{\mathcal{AB}}$ and $t_{yy}^{\mathcal{AB}}$ are unequal in magnitude, similar anisotropies are expected also here.

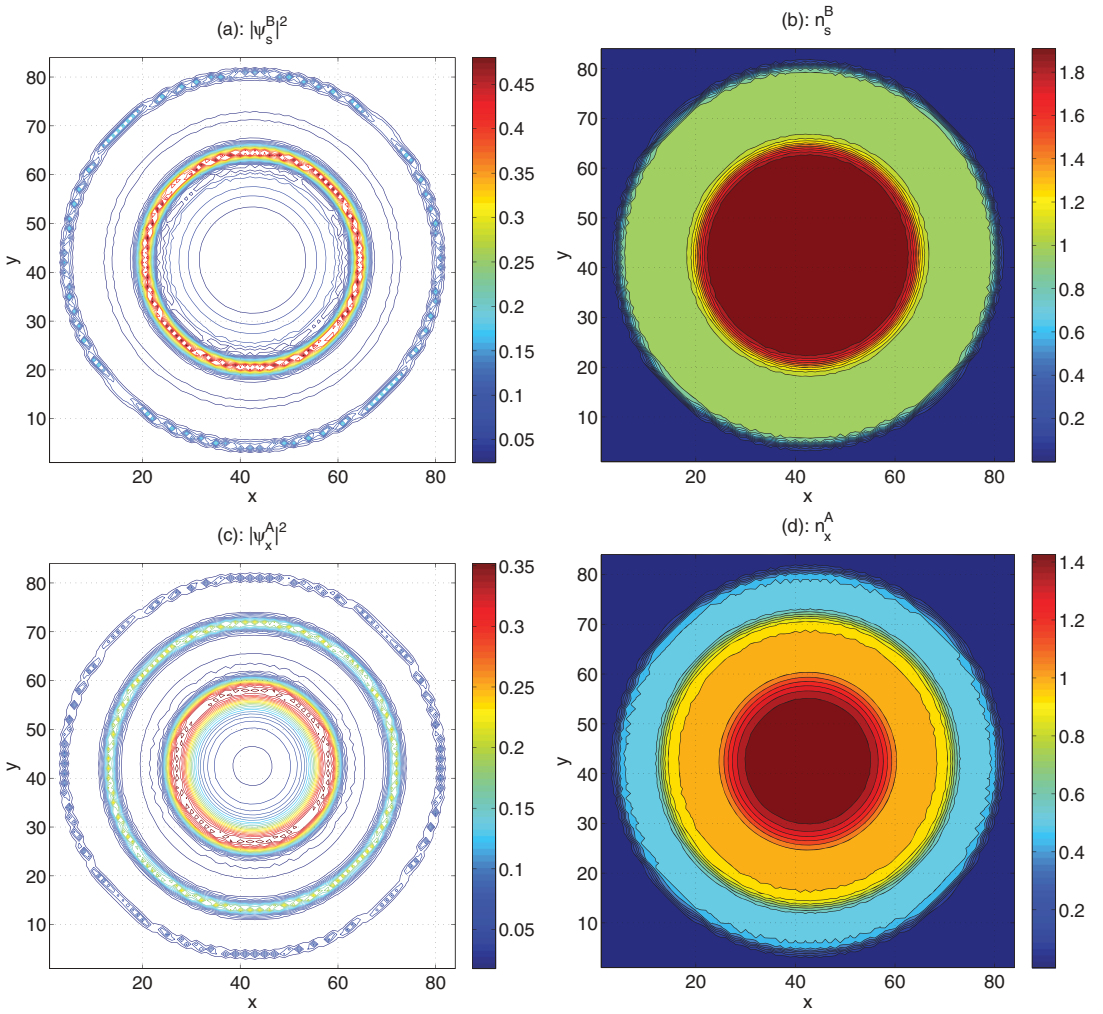

FIG. 6. (Color online) Condensate and flavor densities in a trap. The left hand plots (a) and (b) give the condensate densities $|\langle\hat{\psi}^{\mathcal{B}}_{s,\mathbf{i}}\rangle|^2$ and $|\langle\hat{\psi}^{\mathcal{A}}_{x,\mathbf{i}}\rangle|^2$ while (c) and (d) show atom-flavor densities $n^{\mathcal{B}}_{s,\mathbf{i}}$ and $n^{\mathcal{A}}_{x,\mathbf{i}}$, respectively. We choose $t/U_{s\mathcal{B}} = 0.015$, $\mu_{\text{center}}/U_{s\mathcal{B}} = 1.5$, and γ in such a way that the density vanishes at the edge of the lattice. Since the lattice is isotropic the densities for the y orbital are the same as for the x orbital and are not plotted here. The axes give the lattice sites in the two laboratory directions. (Plotted quantities are only defined in their respective sublattices. However, to make the figure clearer we filled in the relevant values also to the other sublattice by taking the average over the 4 neighboring sites.)

IV. CONCLUSIONS

In this paper we have derived a TB model to describe ultracold atoms in a bipartite optical lattice with three hybridized orbitals. We have also solved the resulting generalized Bose-Hubbard model and found strong modifications to the Mott-insulator-superfluid phase diagram which is found in the simplest lowest-band Bose-Hubbard model. Interesting phenomena were also demonstrated for the confined system that includes a harmonic trap. From that solution we found that the unusual phase diagram of the multiband Bose-Hubbard model can be reflected as possessing a nontrivial wedding-cake structure of Mott insulating regions for different sublattices. In particular, a nonzero condensate order parameter in one sublattice can coexist with a Mott plateau in another sublattice and also appear inside the same Mott plateau. Such effects are observable since Mott insulating regions can be detected *in situ* and atoms in optical lattices can be manipulated even at a single-site resolution [47–50]. Furthermore, since different sublattices have different atom-atom interactions the states with more than one atom per site would generally give rise to different mean-field shifts if transitions to other hyperfine states are considered. This suggest a possibility of addressing different sublattices with microwave fields of different frequencies, for example.

In this paper we have not addressed the dynamical behavior of bosons in a bipartite lattice. However, using the theoretical framework derived here, that would be not only doable, but also interesting since, in the experiments conducted so far, bosons have been initially prepared in an excited state whose dynamical behavior is poorly understood.

ACKNOWLEDGMENTS

Financial support from the Swedish Research Council (Vetenskapsrådet) is acknowledged. J. L. acknowledges

financial support from DAAD (Deutscher Akademischer Austausch Dienst) and the Royal Research Council Sweden (KVA). J. P. M. acknowledges financial support from the Academy of Finland (Project 135646).

[1] D. Jaksch, C. Bruder, J. I. Cirac, C. W. Gardiner, and P. Zoller, Phys. Rev. Lett. **81**, 3108 (1998).
[2] I. Bloch, J. Dalibard, and W. Zwerger, Rev. Mod. Phys. **80**, 885 (2008).
[3] M. Lewenstein, A. Sanpera, V. Ahufinger, B. Damski, A. Sen, and U. Sen, Adv. Phys. **56**, 243 (2007).
[4] M. Greiner, O. Mandel, T. Esslinger, T. W. Hänsch, and I. Bloch, Nature (London) **415**, 39 (2002).
[5] M. L. W. V. Liu, Nature Phys. **7**, 101 (2011).
[6] P. Soltan-Panahi, D.-S. Lühmann, J. Struck, P. Windpassinger, and K. Sengstock, Nature Phys. **8**, 71 (2012).
[7] M. Köhl, K. Günter, T. Stöferle, H. Moritz, and T. Esslinger, J. Phys. B **39**, S47 (2006).
[8] J. Larson, A. Collin, and J.-P. Martikainen, Phys. Rev. A **79**, 033603 (2009).
[9] S. Will, T. Best, U. Schneider, L. Hackermüller, D. Lühmann, and I. Bloch, Nature (London) **465**, 197 (2010).
[10] H. P. Büchler, Phys. Rev. Lett. **104**, 090402 (2010).
[11] K. R. A. Hazzard and E. J. Mueller, Phys. Rev. A **81**, 031602 (2010).
[12] X. Li, E. Zhao, and W. V. Liu, Phys. Rev. A **83**, 063626 (2011).
[13] J. von Stecher, V. Gurarie, L. Radzihovsky, and A. M. Rey, Phys. Rev. Lett. **106**, 235301 (2011).
[14] U. Bissbort, F. Deuretzbacher, and W. Hofstetter, e-print arXiv:1108.6047.
[15] A. Browaeys, H. Häffner, C. McKenzie, S. L. Rolston, K. Helmerson, and W. D. Phillips, Phys. Rev. A **72**, 053605 (2005).
[16] T. Müller, S. Fölling, A. Widera, and I. Bloch, Phys. Rev. Lett. **99**, 200405 (2007).
[17] A. Isacsson and S. M. Girvin, Phys. Rev. A **72**, 053604 (2005).
[18] V. W. Scarola and S. Das Sarma, Phys. Rev. Lett. **95**, 033003 (2005).
[19] V. W. Scarola, E. Demler, and S. Das Sarma, Phys. Rev. A **73**, 051601(R) (2006).
[20] C. Wu, W. V. Liu, J. Moore, and S. Das Sarma, Phys. Rev. Lett. **97**, 190406 (2006).
[21] W. V. Liu and C. Wu, Phys. Rev. A **74**, 013607 (2006).
[22] C. Xu and M. P. A. Fisher, Phys. Rev. B **75**, 104428 (2007).
[23] A. Collin, J. Larson, and J.-P. Martikainen, Phys. Rev. A **81**, 023605 (2010).
[24] G. Wirth, M. Ölschläger, and A. Hemmerich, Nature Phys. **7**, 147 (2011).
[25] M. Ölschläger, G. Wirth, and A. Hemmerich, Phys. Rev. Lett. **106**, 015302 (2011).
[26] M. Ölschläger, G. Wirth, K. Thorge, and A. Hemmerich (2011), e-print arXiv:1110.3716.
[27] A. H. C. Neto, F. Guinea, N. M. R. Peres, K. S. Novoselov, and A. K. Geim, Rev. Mod. Phys. **81**, 109 (2009).
[28] X.-L. Qi and S.-C. Zhang, Rev. Mod. Phys. **83**, 1057 (2011).
[29] L.-K. Lim, C. M. Smith, and A. Hemmerich, Phys. Rev. Lett. **100**, 130402 (2008).
[30] J. Larson, J.-P. Martikainen, A. Collin, and E. Sjöqvist, Phys. Rev. A **82**, 043620 (2010).
[31] V. Apaja, M. Hyrkäs, and M. Manninen, Phys. Rev. A **82**, 041402(R) (2010).
[32] M. Hyrkäs, V. Apaja, and M. Manninen, e-print arXiv:1201.0468.
[33] M. P. Kennett, N. Komeilizadeh, K. Kaveh, and P. M. Smith, Phys. Rev. A **83**, 053636 (2011).
[34] V. S. Shchesnovich, Phys. Rev. A **85**, 013614 (2012).
[35] Z. Cai and C. Wu, Phys. Rev. A **84**, 033635 (2011).
[36] K. Sun, W. V. Liu, A. Hemmerich, and S. Das Sarma, Nature Phys. **8**, 67 (2012).
[37] E. Arimondo, Prog. Opt. **35**, 259 (1996).
[38] K. Bergmann, H. Theuer, and B. W. Shore, Rev. Mod. Phys. **70**, 1003 (1998).
[39] X.-L. Qi, T. L. Hughes, and S.-C. Zhang, Phys. Rev. B **78**, 195424 (2008).
[40] M. Z. Hasan and C. L. Kane, Rev. Mod. Phys. **82**, 3045 (2010).
[41] J. Dalibard, F. Gerbier, G. Juzeliunas, and P. Öhberg, Rev. Mod. Phys. **83**, 1523 (2011).
[42] Y.-J. Lin, K. Jiménez-García, and I. B. Spielman, Nature (London) **471**, 83 (2011).
[43] J. Zakrzewski, Phys. Rev. A **71**, 043601 (2005).
[44] M. P. A. Fisher, P. B. Weichman, G. Grinstein, and D. S. Fisher, Phys. Rev. B **40**, 546 (1989).
[45] F. Pinheiro, J.-P. Martikainen, and J. Larson (2011), e-print arXiv:1111.4633v1.
[46] G. G. Batrouni, V. Rousseau, R. T. Scalettar, M. Rigol, A. Muramatsu, P. J. H. Denteneer, and M. Troyer, Phys. Rev. Lett. **89**, 117203 (2002).
[47] W. S. Bakr, J. I. Gillen, A. Peng, S. Fölling, and M. Greiner, Nature (London) **462**, 74 (2009).
[48] N. Gemelke, X. Zhang, C. Hung, and C. Chin, Nature (London) **460**, 995 (2009).
[49] J. F. Sherson, C. Weitenberg, M. Endres, M. Cheneau, I. Bloch, and S. Kuhr, Nature (London) **467**, 68 (2010).
[50] C. Weitenberg, M. Endres, J. F. Sherson, M. Cheneau, P. Schauß, T. Fukuhara, I. Bloch, and S. Kuhr, Nature (London) **471**, 319 (2011).